In situ observation of the formation, diffusion, and reactions of hydrogenous species in F_2-laser-irradiated SiO_2 glass using a pump-and-probe technique

Koichi Kajihara,[1,*] Linards Skuja,[1,2] Masahiro Hirano,[1] and Hideo Hosono[1,3]
[1]*Transparent Electro-Active Materials Project, ERATO-SORST, Japan Science and Technology Agency, in Frontier Collaborative Research Center, Mail Box S2-13, Tokyo Institute of Technology, 4259 Nagatsuta, Midori-ku, Yokohama 226-8503, Japan*
[2]*Institute of Solid State Physics, University of Latvia, Kengaraga iela 8, LV1063 Riga, Latvia*
[3]*Materials and Structures Laboratory & Frontier Collaborative Research Center, Tokyo Institute of Technology, 4259 Nagatsuta, Midori-ku, Yokohama 226-8503, Japan*
(Received 18 July 2006; published 25 September 2006)

We quantitatively studied the formation, diffusion, and reactions of mobile interstitial hydrogen atoms (H^0) and molecules (H_2) in F_2-laser-irradiated silica (SiO_2) glass between 10 and 330 K. Two key techniques were used: single-pulse F_2 laser photolysis of silanol (SiOH) groups to selectively create pairs of H^0 and oxygen dangling bonds (nonbridging oxygen hole centers, NBOHC), and *in situ* photoluminescence measurements of NBOHCs to monitor their reactions with H^0 and H_2 as a function of time and temperature. A smaller quantum yield of the photolysis of the SiO—H bond (0.15 ± 0.05) compared with values reported for gas molecules containing O—H bonds (~ 1) suggests that the separation of photogenerated H^0 from NBOHC is hindered by the cage effect of the SiO_2 glass network. Distribution functions for the diffusion coefficients of H^0 and H_2 in the structurally disordered SiO_2 glass were evaluated by numerical analysis of the concentration changes of NBOHC based on diffusion-limited reaction theory. The average diffusion coefficient of H_2 obtained by integrating the distribution agrees well with the values measured by the permeation of H_2 through SiO_2 glass plates. In contrast, the average diffusion coefficient of H^0 significantly decreases with time because the distribution of the diffusion coefficient of H^0 is broad and H^0s with greater mobility disappear at a faster rate. We suggest that the efficient conversion of H^0 into H_2 in SiO_2 glass is due to dissipation of the excess energy of the reaction intermediate via inelastic collisions with the glass network. The fraction of H^0 that forms H_2 is determined by the ratio of the capture radii of H^0 and NBOHC, and it is independent of the diffusion coefficient and the initial concentration of H^0.

DOI: 10.1103/PhysRevB.74.094202 PACS number(s): 61.80.Ba, 66.30.Hs, 78.30.Ly, 78.55.Qr

I. INTRODUCTION

High-purity synthetic silica (SiO_2) glass is an important optical material in the deep-ultraviolet (DUV, $h\nu \gtrsim 4$ eV) spectral region because of its excellent transparency for photon energies up to ~ 8 eV and good shape workability. The optical properties of SiO_2 glass in the DUV spectral region are strongly influenced by the presence of interstitial hydrogenous species such as hydrogen atoms (H^0) and molecules (H_2), which are highly mobile and reactive chemical species in SiO_2 glass. The incorporation of H_2 in SiO_2 glass is effective in improving transmittance at $\sim 4-7$ eV. This improvement is mainly due to elimination of silicon dangling bonds ($\equiv Si^{\bullet}$, "E' centers"), oxygen dangling bonds ($\equiv SiO^{\bullet}$, "nonbridging oxygen hole centers," NBOHC), and divalent Si ["ODC(II)"] by reactions with H^0 and H_2.[1–9] High-temperature thermal annealing of SiO_2 glass in H_2 decomposes preexisting oxygen vacancies [Si—Si bonds, "ODC(I)"], which exhibit an intense absorption band at 7.6 eV.[10,11] However, interstitial H_2 can also act detrimentally as it slowly dissociates Si—O bonds to form pairs of hydroxyl (SiOH) and hydride (SiH) groups.[12–15] The formation of SiOH groups by this mechanism is responsible for degradation of the infrared transmittance of SiO_2-based optical telecommunication fibers ("hydrogen corrosion").[16–20] Another significant reaction is the photoreduction of Si—O—Si bonds to Si—Si bonds under excitation with ArF ($h\nu$=6.4 eV) or F_2 ($h\nu$=7.9 eV) laser light,[21] showing a striking contrast to the case of high-temperature thermal annealing in H_2.[10,11] The photoreduction is accompanied by the formation of macroscopic cracks,[21] probably due to stress corrosion[22,23] of the Si—O—Si network by photogenerated H_2O. H_2-loaded SiO_2 glasses also undergo a radiation-induced expansion, resulting in a decrease in the refractive index, as opposed to the radiation-induced densification in H_2-free SiO_2 glasses.[24–26]

In general, the rate-limiting step of reactions involving mobile hydrogenous species in SiO_2 glass is diffusion of the hydrogenous species to reaction sites.[27,28] Their diffusion in SiO_2 glass has therefore been studied in detail.[13,19,27,29–45] One of the most commonly used methods to evaluate the diffusion of these species close to and below room temperature is to create H^0 via the radiolysis of preexisting SiOH and SiH groups using x rays, γ rays, electron-beam or UV laser pulses, and to measure the concentration changes of radiation-induced defects *in situ* by electron paramagnetic resonance (EPR),[27,37–40,43,45] or by measurements of optical absorption and photoluminescence.[6–8,36,46–49] These previous studies have confirmed that in SiO_2 glasses containing SiOH groups ("wet" SiO_2 glasses), the mobile H^0 and H_2 participate in the following reactions:

$$\equiv SiO^{\bullet} + H^0 \rightarrow \equiv SiOH, \quad (1)$$

$$\equiv SiO^{\bullet} + H_2 \rightarrow \equiv SiOH + H^0, \quad (2)$$

$$2H^0 \rightarrow H_2. \quad (3)$$

However, ionizing radiation or multiphoton excitation with UV laser pulses dissociate the SiO—H bonds at relatively low rates. In addition to the SiO—H bonds, other chemical bonds are also cleaved. Analysis of such a system is complicated because the processes of SiO—H breaking and recovery overlap, and mobile H^0 and H_2 can be trapped by additional defects created by the irradiation. There was also a lack of sensitive spectroscopic techniques that are capable of measuring the concentration of defects in a short time and over a wide range of temperatures. Thus it has previously been difficult to accurately evaluate the mobility of H^0 and H_2 that participate in radiation-induced processes.

In previous studies, we developed an F_2-laser-based pump-and-probe method to monitor the mobile interstitial H^0 and H_2 *in situ*.[50,51] Excitation of the optical-absorption band of SiOH groups [>7.3 eV (Refs. 52–55)] with F_2 laser light dissociates the SiO—H bonds with a quantum yield (Φ) of $\gtrsim 0.1$,[50,56] which is much larger than that of other competitive processes, such as the dissociation of Si—O bonds [$\Phi \sim 10^{-4}$ (Refs. 50 and 57)]. This enables the selective creation of as many as $\sim 10^{16}$ cm^{-3} pairs of H^0 and NBOHC with a single F_2 laser pulse. The concentration of NBOHC was measured down to $\sim 10^{14}$ cm^{-3} in a very short time (~ 10 μs) from its laser-induced 1.9-eV photoluminescence (PL), which is detectable at all temperatures below ~400–500 K.[58] This technique is particularly useful at temperatures above ~200 K where the detection of NBOHC by EPR is made difficult by line broadening.[59]

The local diffusivity of mobile species in SiO_2 glass is inevitably nonuniform because they traverse interstitial voids of various shapes and sizes.[27,34,45,51] We evaluated the activation energy required for the diffusion of H^0 and H_2 by taking into account the distribution arising from the structural disorder of SiO_2 glass. The activation energy was evaluated by numerically simulating the NBOHC decay curves associated with the reactions Eqs. (1)–(3). The results were reported briefly in the preceding Letter.[51] The current paper presents a detailed analysis of the diffusion of H^0 and H_2 in SiO_2 glass. We discuss the influence of interstitial voids on the formation, diffusion, and reactions of mobile H^0 and H_2.

II. EXPERIMENTAL PROCEDURE

A. Measurements

We used synthetic wet SiO_2 glass plates ($10 \times 10 \times 1$ mm^3) that contain SiOH groups at a concentration of $\sim 1.0 \times 10^{20}$ cm^{-3} (evaluated using an absorption cross section[54] reported for the infrared-absorption band at ~ 3675 cm^{-1}). The glass also contained interstitial H_2 molecules[51] of unknown concentration and spatial distribution, and $\sim 5 \times 10^{18}$ cm^{-3} impurity chloride (SiCl) groups.[82] This preexisting H_2 was removed by thermal annealing for 4 h at 800 °C, yielding an H_2-free sample. An H_2-loaded sample with a homogenous H_2 distribution was prepared by heating the H_2-free sample in H_2 (~2.3 atm) for 12 h at 500 °C. The H_2 concentration, evaluated using solubility data for H_2 in SiO_2 glass,[30] was $\sim 5 \times 10^{17}$ cm^{-3}.

To measure changes in the concentration of NBOHC, we used the same procedure as that described in the preceding report.[51] The sample set in a cryostat was exposed to F_2 laser pulses (energy density, ~30 mJ cm^{-2} pulse^{-1}; pulse duration, ~20 ns; Model LPF-210, Lambda Physik) to create NBOHC and H^0 ($\sim 10^{16}$–10^{17} cm^{-3} per pulse) by dissociating the SiO—H bonds. The subsequent NBOHC decay associated with reactions with H^0 or H_2 [Eqs. (1)–(3)] was monitored by the intensity of the 1.9-eV PL band of NBOHC. The PL band was excited in the 4.8-eV absorption band of NBOHC,[60] with repetitive probe pulses from a frequency-quadrupled Nd:YAG laser ($h\nu$=4.7 eV; ~0.1 mJ cm^{-2} pulse^{-1}; 2 s intervals; Model INDI, Spectra Physics). To avoid interference from F_2-laser-induced 1.9 eV PL,[61] the first probe pulse after the creation of NBOHC was delayed by t_D (typically 1 ms) compared to the first F_2 laser pulse irradiated at t=0. The PL intensity was converted to NBOHC concentration using the procedure described in Secs. III A–III C. The experimental setup and pulse sequence are shown schematically in Ref. 50.

B. Data analysis

The experimental decay curves of NBOHC concentrations were simulated by solving simultaneous differential rate equations derived from Eqs. (1)–(3),

$$\frac{d}{dt}[\mathrm{NBOHC}] = -k_1[\mathrm{NBOHC}][H^0] - k_2[\mathrm{NBOHC}][H_2], \quad (4)$$

$$\frac{d}{dt}[H^0] = -k_1[\mathrm{NBOHC}][H^0] + k_2[\mathrm{NBOHC}][H_2] - k_3[H^0]^2, \quad (5)$$

$$\frac{d}{dt}[H_2] = -k_2[\mathrm{NBOHC}][H_2] + \frac{k_3}{2}[H^0]^2, \quad (6)$$

where the concentration of each species is denoted by square brackets. Since the reactions Eqs. (1)–(3) are diffusion-limited,[27,28] the reaction rate constants k_1, k_2, and k_3 can be expressed by[62]

$$k_1 = 4\pi r_1 D_{H^0}\left(1 + \frac{r_1}{\sqrt{\pi D_{H^0} t}}\right), \quad (7)$$

$$k_2 = 4\pi r_2 D_{H_2}\left(1 + \frac{r_2}{\sqrt{\pi D_{H_2} t}}\right), \quad (8)$$

$$k_3 = 8\pi r_3 D_{H^0}\left(1 + \frac{r_3}{\sqrt{2\pi D_{H^0} t}}\right), \quad (9)$$

where D_{H^0} and D_{H_2} are the diffusion coefficients of H^0 and H_2, respectively. r_1, r_2, and r_3 are the capture radii, within which the reaction is assumed to be completed immediately, and no interactions propagate beyond that distance. The cap-

ture radii for reactions involving NBOHC, r_1 and r_2, were set to 0.5 nm following Ref. 27. The capture radius for the dimerization of H^0, r_3, was determined using the procedure described in Sec. III D.

It was assumed that each D depends on temperature T following the Arrhenius law,

$$D = D_0 \exp(-E_a/k_B T), \tag{10}$$

where E_a, D_0, and k_B are the activation energy, preexponential factor and the Boltzmann constant, respectively. The effect of the structural disorder of SiO_2 glass on the diffusion of H^0 and H_2 was approximately accounted for by introducing distribution functions of E_a.[27,34] The unknown distribution functions for H^0 and H_2, $w_{H^0}(E_a)$, and $w_{H_2}(E_a)$, were numerically represented by N_{H^0} and N_{H_2} sample points taken at discrete values of E_a, respectively. The observed diffusion process was treated as a superposition of N_{H^0} times N_{H_2} separate diffusion processes, each characterized by a pair of the discrete activation energy values for the diffusion of H^0 and H_2. It was assumed that cross correlations between $w_{H^0}(E_a)$ and $w_{H_2}(E_a)$ are absent.

The rate equations Eqs. (4)–(6) were solved for each of $N_{H^0}N_{H_2}$ processes. A linear combination of the solutions was calculated by multiplying with their statistical weights $w_{H^0}(E_{a,i})w_{H_2}(E_{a,j})$, which satisfies $\Sigma_{i=1}^{N_{H^0}} w_{H^0}(E_{a,i})=1$ and $\Sigma_{j=1}^{N_{H_2}} w_{H_2}(E_{a,j})=1$. It was fitted to the experimental decay curves, regarding the values of coefficients $w_{H^0}(E_{a,i})$ and $w_{H_2}(E_{a,j})$ as fitting parameters. However, the number of independent fitting parameters, $(N_{H^0}-1)(N_{H_2}-1)$, was too large to yield a unique fit. To reduce the number of parameters, $w(E_a)$ was approximated using a combination of analytical peak functions that were permitted to be asymmetric against the peak positions. We employed an asymmetric Gaussian function characterized by parameters of a, b, c, and d,

$$f_{AG}(E_a) = a \exp\left[-\left(\frac{E_a - b}{g}\right)^2\right],$$
$$\text{where } g = \begin{cases} 2c/[1+\exp(d)] & (E_a \geqq b) \\ 2c/[1+\exp(-d)] & (E_a < b) \end{cases}. \tag{11}$$

The asymmetry parameter d, which is zero for the conventional Gaussian function, can be varied without changing the peak half width and area. The E_a values at the peak position and at the half maxima are given by

$$E_a^{max} = b, \tag{12}$$

$$E_a^{HM\text{-}low} = b - 2c(\ln 2)^{1/2}/[1+\exp(-d)], \tag{13}$$

$$E_a^{HM\text{-}high} = b + 2c(\ln 2)^{1/2}/[1+\exp(d)], \tag{14}$$

and the full width at the half maximum (FWHM) is equal to $E_a^{HM\text{-}high} - E_a^{HM\text{-}low} = 2c(\ln 2)^{1/2} = 1.665c$.

The quantum yield of NBOHC formation Φ was derived from the observed concentration of NBOHC created by a single F_2 laser pulse $C_{0,exp}$ using

$$\Phi = \frac{LC_{0,exp}}{J} \frac{1 - r\exp(-\alpha L)}{(1-r)[1-\exp(-\alpha L)]}, \tag{15}$$

where L is the sample thickness ($L=1$ mm), α is the temperature-dependent absorption coefficient at 7.9 eV determined in Ref. 63, J is the photon fluence of an F_2 laser pulse ($\sim 2.4\times 10^{16}$ cm^{-2} at 30 mJ cm^{-2} pulse^{-1}) and r is the reflection on each surface [$r=(1-n)^2/(1+n)^2$ where n is the refractive index ($n=1.69$ at 7.9 eV, Ref. 64)]. It was assumed that α characterizes the optical absorption of SiOH groups and that the contribution from the fundamental absorption of SiO_2 glass is negligible.[63,65] The detailed procedure involved in determining Φ is described in Sec. III C.

The initial NBOHC concentration used for the simulation was obtained from Φ, while taking into consideration the macroscopic concentration gradient along the thickness of the sample related to attenuation of the F_2 laser light. The initial concentration of NBOHC formed in the layer defined by the distances from the irradiated surface, L_1 and L_2 ($0 \leqq L_1 < L_2 \leqq L$), was obtained by

$$C_0(L_1,L_2) = \frac{J\Phi}{L_2 - L_1} \frac{1-r}{1-r^2\exp(-2\alpha L)} \times \{\exp(-\alpha L_1) - \exp(-\alpha L_2) - r\exp[-\alpha(2L-L_1)] + r\exp[-\alpha(2L-L_2)]\}. \tag{16}$$

The sample was treated as consisting of five layers, each with a thickness of 0.2 mm. The NBOHC decay in each layer was calculated independently at different $C_0(L_1,L_2)$ and the results were averaged. The calculated decay was least-squares fitted to the experimental decay curves by adjusting D_{0,H^0} and D_{0,H_2} as well as the peak parameters a, b, c, and d associated with $w_{H^0}(E_a)$ and $w_{H_2}(E_a)$.

III. RESULTS

A. Temperature ranges of the diffusion of H^0 and H_2

Figure 1 shows temperature-dependent decay curves of the normalized concentrations of NBOHC ([NBOHC]/C_0 where $C_0 \equiv C(0,L)$) in the H_2-free and H_2-loaded samples exposed to a single F_2 laser pulse at 10 K ("thermal decay experiment"). The decay curves were obtained as follows. The irradiated sample was first held for 500 s at 10 K and then heated to 330 K at a constant rate of 3 K min^{-1} while recording the intensity of the 1.9 eV PL of NBOHC, $I(T,t)$. A small amount of NBOHC remained in the H_2-free sample at 330 K. This sample was cooled to 10 K once more and was subjected to the same heating program to record the PL intensity, $Q(T)$, without irradiation with the F_2 laser pulse. Because the NBOHC concentration was constant during the second temperature sweep, $Q(T)$ corresponds to the temperature dependence of the PL intensity. Thus the concentration decay curves shown in Fig. 1 are given by $[\text{NBOHC}]/C_0 = I(T,t)/I(10\text{ K},0)\times Q(10\text{ K})/Q(T)$.

Figure 2 shows time-dependent decay curves of the normalized concentrations of NBOHC in the H_2-free sample

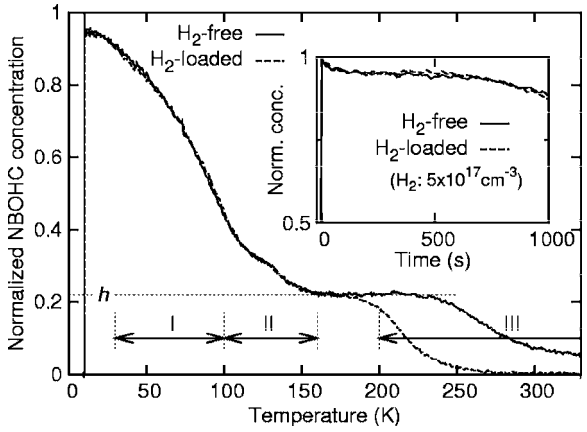

FIG. 1. Temperature-dependent decay curves of the normalized NBOHC concentration in the H_2-free and H_2-loaded samples measured under a constant heating rate of 3 K min^{-1} (thermal decay experiment). The subvertical line near $t=0$ corresponds to data points measured after a delay of $t_D=1$ ms from the F_2 laser pulse that causes the photolysis ($t=0$). The subsequent sampling interval was 2 s. The decay can be separated into three temperature ranges: I, <100 K; II, 100–160 K; and III, >200 K. The normalized height of the plateau between ranges II and III is denoted by h and used in Eq. (24). The inset shows the NBOHC decay curves plotted with respect to time. The temperature of the sample was held at 10 K until $t=500$ s and then raised by 3 K min^{-1}.

exposed to an F_2 laser pulse under a constant temperature between 60 and 300 K ("isothermal decay experiment"). Here, the recorded PL intensity $I_T(t)$ is simply proportional to the concentration of NBOHC. Thus the decay curves shown in Fig. 2 are given by $[\text{NBOHC}]/C_0=I_T(t)/I_T(0)$.

In the cases of both Figs. 1 and 2, the decay of NBOHC can be separated into three temperature ranges: I (<100 K), II (~100–160 K), and III (>200 K). Decay of NBOHC in ranges I and II is due to the reaction Eq. (1) with H^0.[36–40,51]

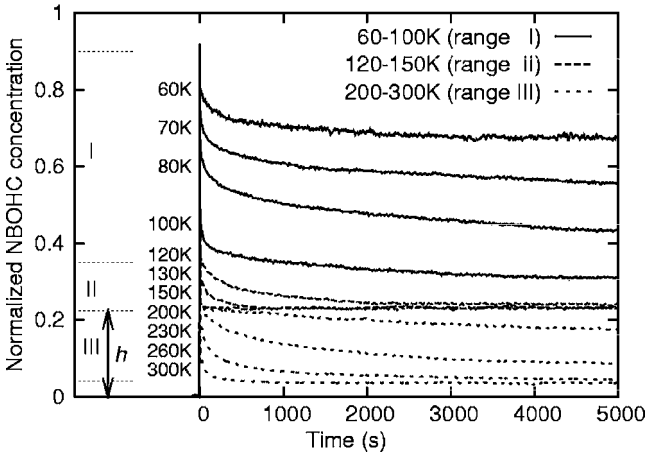

FIG. 2. Time-dependent decay curves of the normalized NBOHC concentration in the H_2-free samples measured under constant temperatures (isothermal decay experiment). On the basis of the data shown in Fig. 1, the decay curves are divided into three groups: I, II, and III. The normalized height of the plateau between ranges II and III is denoted by h.

Range III is due to the reaction Eq. (2) with H_2 followed by the secondary reaction Eq. (1).[27,28,45,51]

In each of the temperature ranges (I, II, and III), the distribution of E_a was approximated by the unimodal function, as given by Eq. (11). Thus $w_{H^0}(E_a)$ and $w_{H_2}(E_a)$ were modeled by bimodal and unimodal functions, respectively. The sample points were set between 0.01 and 0.32 eV in 0.01 eV steps for $w_{H^0}(E_a)$ ($N_{H^0}=32$), and between 0.26 and 0.56 eV in 0.02 eV steps for $w_{H_2}(E_a)$ ($N_{H_2}=16$).

B. Initial concentrations of NBOHC and H^0

The absolute concentrations of NBOHC created by a single F_2 laser pulse $C_{0,\text{exp}}$ were evaluated at temperatures of $T=10$, 50, 100, 150, 200, 250, and 300 K by measuring the intensity of the associated 4.8-eV optical-absorption band, for which the peak absorption cross section σ is known [5.3×10^{-18} cm^2 (Ref. 60)]. This was implemented by relating the induced 4.8-eV absorption and 1.9-eV PL band intensities, because direct *in situ* measurement of the absorption band induced by an F_2 laser pulse was not possible due to its low intensity and restrictions related to the experiment geometry. An H_2-free sample was exposed at each T to a single F_2 laser pulse, and the intensity of the induced 1.9 eV PL $I(T,t_D)$ was registered at $t_D=200$ μs or 1 ms. The sample was then further exposed to 99-F_2 laser pulses and warmed up in the usual way. At the end of the temperature sweep at 330 K, the PL intensity $I(330\text{ K},t_{\text{end}})$ was recorded and the sample was rapidly cooled to room temperature. This treatment generated a significant room-temperature-stable 4.8-eV absorption band of NBOHC,[51,66,67] whose absorption coefficient α was accurately measured by transferring the sample to a conventional spectrometer (U-4000, Hitachi). The concentration of NBOHC created by the first F_2 laser pulse at T was calculated as

$$C_{0,\text{exp}}=\frac{I(T,t_D)}{I(330\text{ K},t_{\text{end}})}\frac{Q(330\text{ K})}{Q(T)}\frac{\alpha}{\sigma}, \tag{17}$$

where $Q(T)$ is the characteristic temperature dependence of the PL intensity caused by the thermal quenching, as determined in Sec. III A. This procedure made it possible to calibrate the relation between the NBOHC concentration and the PL intensity using a *single* sample, thus avoiding errors introduced by different geometric factors and uncertainties in the accuracy of sample re-insertion. The typically observed $C_{0,\text{exp}}$ values, averaged over the thickness direction, were $\sim2\times10^{16}$ cm^{-3} per F_2 laser pulse of ~30 mJ cm^{-2}.

The inset of Fig. 1 shows that the NBOHC concentration decreased slightly at 10 K over the first 500 s, prior to the start of the temperature sweep. Figures 1 and 2 show a plateau of nonzero NBOHC concentration at the end of the measurements above 300 K. These two observations were modeled by assuming that 5% of H^0 recombines with NBOHC prior to the beginning of the thermal decay, and that 4% of H^0 takes part in reactions other than those described in Eqs. (1)–(3); for example, photoassisted cracking of Si—O bonds with H^0,[66,67] and generation of interstitial HCl from

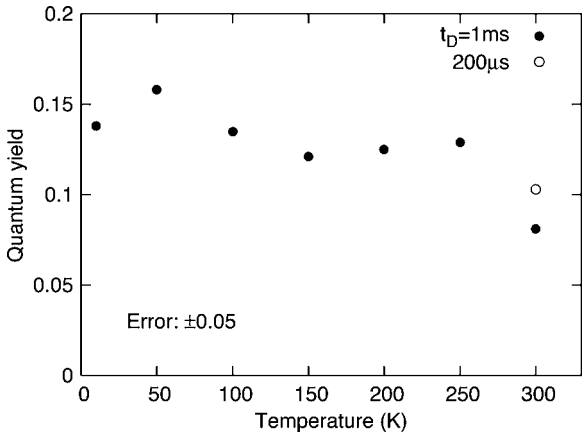

FIG. 3. Temperature dependence of the measured quantum yield of NBOHC formation, Φ_{exp}, calculated via Eq. (15) using H_2-free samples exposed to 100 F_2 laser pulses between 10 and 300 K. The detailed procedure of the calculation is described in the text. The typical delay of the probe pulse from the F_2 laser pulse was t_D =1 ms (filled circles). For comparison, an additional data point was measured for t_D=200 μs at 300 K (open circle).

SiCl groups.[82] Thus the initial concentrations of NBOHC and H^0 used for the calculations were $[NBOHC]_0=0.95C_0$ and $[H^0]_0=0.91C_0$, respectively.

C. Quantum yield of NBOHC formation

To determine the initial NBOHC concentration $C_0 \equiv C_0(0,L)$ and the depth distribution $C_0(L_1,L_2)$ from Eq. (16), the photolysis quantum yield Φ must first be evaluated. Its experimentally measured value, Φ_{exp}, was obtained via Eq. (15). However, C_0 is defined as the NBOHC concentration immediately following the F_2 laser pulse (t=0), whereas $C_{0,exp}$ was measured after a delay of t_D. Hence $C_{0,exp}$ is evidently smaller than C_0 because of the concentration decay of NBOHC during t_D, yielding a value of Φ_{exp} that is somewhat smaller than the true quantum yield Φ.

The temperature dependence of Φ_{exp} is shown in Fig. 3. The annihilation of NBOHC during t_D is considered to be negligible at 10 K because of the very low mobility of H^0 and H_2. In addition, Φ_{exp} measured at t_D=1 ms was almost constant between 10 and 250 K, suggesting that NBOHC decay during t_D is not significant, even at 250 K. The slight decrease in Φ_{exp} at 300 K is evidently due to the recombination of NBOHC with H^0 and H_2 during t_D. Indeed, Φ_{exp} increased with decreasing t_D from 1 ms to 200 μs. Hence it seems likely that Φ is approximately equal to Φ_{exp} and is almost constant at a value of 0.15±0.05 between 10 and 300 K. In this simulation, Φ was fixed at 0.15.

D. Branching ratio of reactions that consume H^0

The photogenerated H^0 is consumed by two parallel reactions Eqs. (1) and (3) in temperature ranges I and II (<160 K). Since the initial concentrations of NBOHC and H^0 are similar and only the reaction Eq. (1) annihilates NBOHC, the normalized height of the plateau between ranges II and III, h, in Figs. 1 and 2, is related to the branching ratio between these reactions. The h value determined from Figs. 1 and 2 was ~0.22.

Below 160 K, H_2 is almost immobile ($D_{H_2}\sim 0$) and k_2 defined by Eq. (8) is ~0. Equations (4) and (5) are then simplified as

$$\frac{d}{dt}[\mathrm{NBOHC}] = -k_1[\mathrm{NBOHC}][\mathrm{H}^0], \tag{18}$$

$$\frac{d}{dt}[\mathrm{H}^0] = -k_1[\mathrm{NBOHC}][\mathrm{H}^0] - k_3[\mathrm{H}^0]^2. \tag{19}$$

[NBOHC] and $[H^0]$ can be replaced by the respective normalized concentrations, $[NBOHC]/C_0 \equiv x$ and $[H^0]/C_0 \equiv y$, where x and y vary between 0 and 1 (initial values: x_0 and y_0). Provided that the second terms in Eqs. (7) and (9) are negligible on the time scale of this study, Eqs. (18) and (19) become

$$dx = -4\pi D_{H^0} C_0 r_1 xy dt, \tag{20}$$

$$dy = -4\pi D_{H^0} C_0 (r_1 x + 2r_3 y) y dt. \tag{21}$$

Division of Eq. (21) by Eq. (20) shows a direct relation between x and y that is only parametrically dependent on t,

$$\frac{dy}{dx} = 1 + \gamma\frac{y}{x} \equiv \frac{1}{p}, \tag{22}$$

where $\gamma \equiv 2r_3/r_1$. The value $p=dx/dy$ represents the branching ratio: the probability that an interstitial H^0 reacts directly with NBOHC [Eq. (1)] rather than undergoing dimerization to H_2 [Eq. (3)]. The probability increases from $p_0=(1+\gamma y_0/x_0)^{-1}$ to 1 with t, indicating that the recombination of H^0 with NBOHC [Eq. (1)] becomes more probable than the dimerization of H^0s [Eq. (3)] as the concentration of H^0 becomes smaller than that of NBOHC. The solution of Eq. (22) is

$$y = \left(\frac{x}{x_0}\right)^{\gamma}\left(y_0 + \frac{x_0}{\gamma - 1}\right) - \frac{x}{\gamma - 1}. \tag{23}$$

It is clear that the relation between x and y is influenced by γ but is independent of C_0 and D_{H^0}.

At 160 K, where H^0s completely disappear (y=0), x is equal to h (Figs. 1 and 2). Thus h is related to γ via Eq. (23) as

$$h = \left[\frac{\gamma - 1}{x_0^{\gamma}}\left(y_0 + \frac{x_0}{\gamma - 1}\right)\right]^{1/(1-\gamma)}. \tag{24}$$

Substitutions of h=0.22, x_0=0.95, and y_0=0.91 into Eq. (24) yielded $\gamma\sim 0.38$. Using r_1=0.5 nm,[27] $r_3=r_1\gamma/2$ was determined to be ~0.095 nm.

The integrated branching ratio (ratio of the integrated concentration changes of H^0 and NBOHC below 160 K), p_I, is defined by

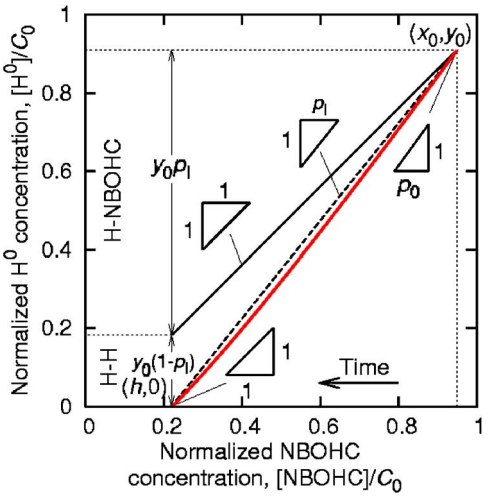

FIG. 4. (Color online) Calculated relation between the normalized concentrations of NBOHC ($[\mathrm{NBOHC}]/C_0 \equiv x$) and H^0 ($[H^0]/C_0 \equiv y$) during the NBOHC decay in ranges I and II below 160 K, obtained via Eq. (23) (thick colored line). The decay starts at the point (x_0,y_0) and finishes at the point $(h,0)$. Substitutions of parameters $x_0=0.95$, $y_0=0.91$, and $h=0.22$ obtained experimentally from Fig. 1 into Eq. (23) yield the locus of points (x,y) (thick colored line) and the ratio of the capture radii of NBOHC and H^0, $\gamma=2r_3/r_1=0.38$. The initial concentration of NBOHC, C_0, and the diffusion coefficient of H^0, D_{H^0}, do not influence the locus, but determine the movement rate of the point (x,y). The branching ratio (probability that an interstitial H^0 reacts with NBOHC rather than with reacting another H^0 to form H_2) at each point (x,y) is given by $p=(1+\gamma y/x)^{-1}$ [Eq. (22)]. The integrated branching ratio p_I is equal to the inverse of the slope of the dashed line connecting the points (x_0,y_0) and $(h,0)$ [Eq. (25)]. Thin line that connects the points (x_0,y_0) and $[h,y_0(1-p_I)]$ with slope 1 separates H^0s used for these two reactions.

$$p_I = \frac{[\mathrm{NBOHC}]_0 - [\mathrm{NBOHC}]_{160\ \mathrm{K}}}{[\mathrm{H}^0]_0 - [\mathrm{H}^0]_{160\ \mathrm{K}}} = \frac{x_0 - h}{y_0}, \qquad (25)$$

where $[\mathrm{NBOHC}]_{160\ \mathrm{K}}$ and $[\mathrm{H}^0]_{160\ \mathrm{K}}$ denote the respective concentrations at 160 K. The calculated p_I value was ~0.80. Figure 4 summarizes the correlations among the parameters x, y, h, p, and p_I.

The above observation demonstrates that the branching ratio of reactions Eqs. (1) and (3) is determined by the ratio of the capture radii between H^0 and NBOHC.

E. Simulation of NBOHC decay at constant temperatures

Figure 5 shows isothermal NBOHC decay curves for the H_2-free samples at 100 and 260 K plotted against a logarithm of time. Dashed lines in Fig. 5 are simulated curves calculated at different discrete E_a values without considering the E_a distribution. None of the curves show a good fit with the experimental decay curves. However, it is possible to improve the goodness of fit by taking a linear combination of the simulated curves using $w(E_a)$ as the weighting function.[27,34] This procedure was used to determine D_{0,H^0}, D_{0,H_2}, $w_{H^0}(E_a)$, and $w_{H_2}(E_a)$. The uncertainty in the values of these parameters was significantly reduced by *simultaneously* fitting the full set of experimental curves taken at different temperatures.

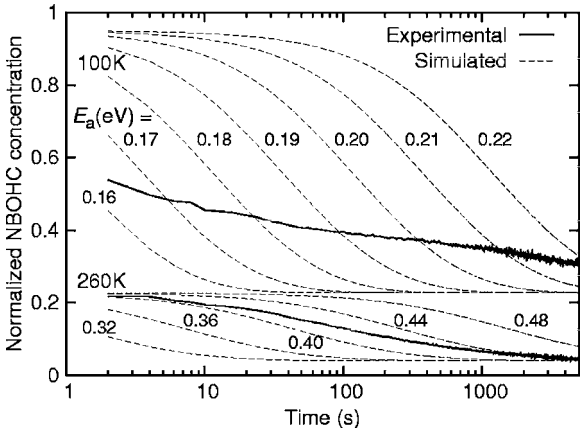

FIG. 5. Isothermal decay curves of the normalized NBOHC concentration in the H_2-free sample at 100 and 260 K (solid lines) and simulated curves calculated at several definite values of activation energies for diffusion (E_a) at 100 K for H^0 and 260 K for H_2 (dashed lines).

The actual calculation was performed as follows. First, decay curves in ranges I and II (<200 K) associated with reactions Eqs. (1) and (3) were simulated using Eqs. (18) and (19). All the decay curves in ranges I and II were simultaneously fitted by treating D_{0,H^0} and $w_{H^0}(E_a)$ as common fitting parameters. Then, fixing D_{0,H^0} and $w_{H^0}(E_a)$ at these values, the decay curves in range III were simulated using Eqs. (4)–(6) by adjusting D_{0,H_2} and $w_{H_2}(E_a)$. The fitting result is shown in Fig. 6. The best-fit values were $D_{0,H^0} \sim 4.3 \times 10^{-3}$ and $D_{0,H_2} \sim 8.5 \times 10^{-5}$ cm^2 s^{-1}, and the obtained $w(E_a)$ are presented in Sec. III G.

F. Simulation of NBOHC decay under a constant heating rate

Figure 7 shows the thermal NBOHC decay curve of the H_2-free sample measured under a constant heating rate. In a similar way to the procedure described in Sec. III E, the ex-

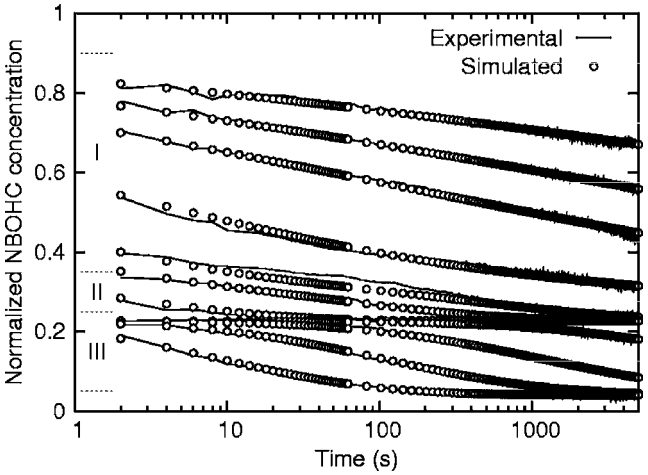

FIG. 6. Simulated isothermal decay curves of normalized NBOHC concentration calculated using the E_a distribution shown in Fig. 9 (open symbols). Experimental decay curves (solid lines) are identical to those shown in Fig. 2.

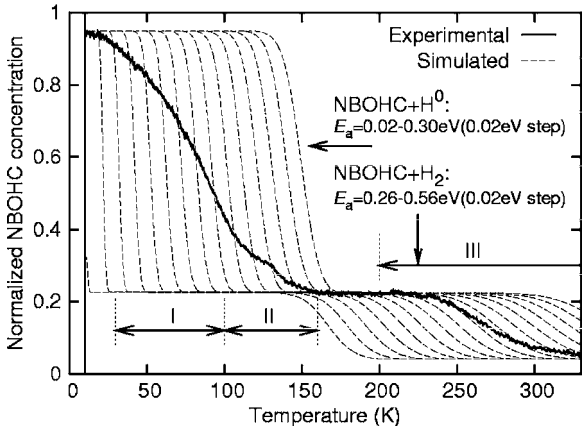

FIG. 7. Thermal decay curves of the normalized NBOHC concentration in the H_2-free sample measured under a constant heating rate of 3 K min^{-1} (solid line) and simulated curves calculated at several definite values of E_a for the diffusion of H^0 and H_2 (dashed lines).

perimental decay curve was simulated by a linear combination of decay curves calculated for different E_a values. However, it was not possible to determine a unique pair of D_0 and $w(E_a)$ solely from the two available decay curves for the H_2-free and H_2-loaded samples (Fig. 1). Hence D_{0,H^0} and D_{0,H_2} were fixed at the values already obtained in Sec. III E, and the two decay curves were simultaneously simulated using $w_{H^0}(E_a)$ and $w_{H_2}(E_a)$ as common optimizing parameters. The experimental and simulated results are in good agreement (Fig. 8). The inset of Fig. 8 shows the simulated concentration changes of NBOHC, H^0, and H_2 in the H_2-free sample. This figure clearly shows the simultaneous reaction of H^0 with NBOHC [Eq. (1)] and formation of H_2($\sim 3 \times 10^{15}$ cm^{-3}) [Eq. (3)] below 160 K.

G. Distribution of activation energy for diffusion

Figure 9 shows $w(E_a)$ obtained from the isothermal decay

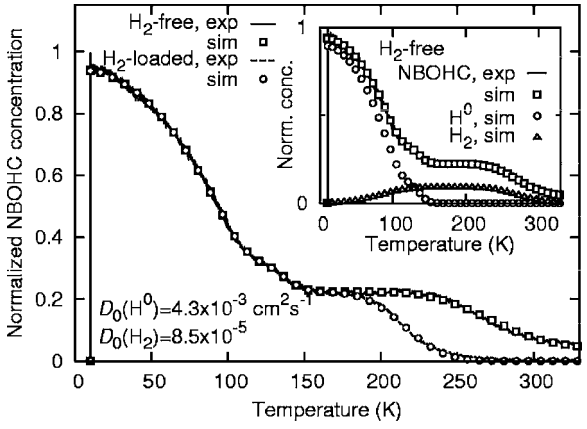

FIG. 8. Thermal decay curves of the normalized NBOHC concentration in the H_2-free and H_2-loaded samples measured under a constant heating rate of 3 K min^{-1} (solid and dashed lines, respectively) and simulated curves calculated using the E_a distribution shown in Fig. 9 (open symbols). The inset shows the simulated curves of the normalized concentrations of NBOHC, H^0, and H_2 in the initially H_2-free sample.

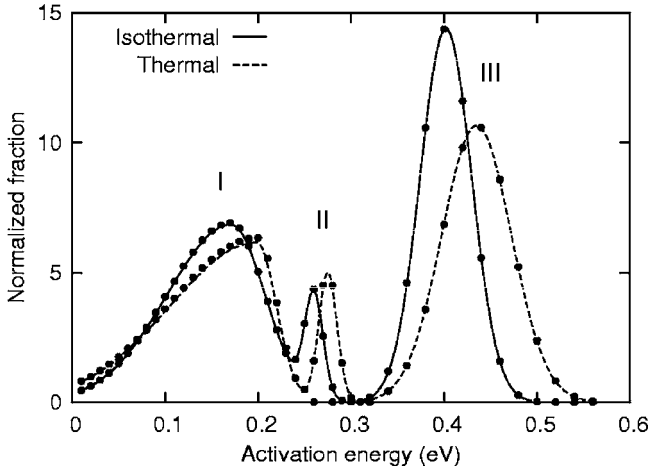

FIG. 9. Calculated distribution of activation energy for the diffusion, E_a, of H^0 (ranges I and II) and H_2 (range III), used to obtain the simulated NBOHC decay curves shown in Figs. 6 and 8. Filled symbols denote the discrete E_a values used in the simulation.

(Fig. 6) and thermal decay (Fig. 8) experiments. An asymmetric Gaussian function was necessary to describe $w(E_a)$ in range I, whereas symmetric Gaussian functions provided a good results for ranges II and III. Since $w(E_a)$ distributions obtained from the isothermal and thermal decay experiments agree reasonably well, only their average peak parameters are considered in the following discussion. The centers of gravity for the distribution peaks I, II, and III were located at ~0.16, ~0.27, and ~0.42 eV, respectively.

IV. DISCUSSION

Since the electronic structure of OH groups is generally insensitive to the chemical structures attached to them, the photolysis properties of the O—H bond are expected to be similar among compounds containing OH groups. The lowest electronic excited state of an OH group, which is generally located at ~6–7 eV above the ground state, is repulsive against the stretching of an O—H bond. The photolysis is therefore very efficient for an isolated molecule in a vapor phase [overall quantum yield $\Phi \sim 1$ (H_2O) (Ref. 68) and 0.86 ± 0.10 (CD_3OH) (Ref. 69)]. However, Φ of the photolysis of H_2O in a rare-gas matrix is as small as $\lesssim 0.6$, and the threshold photon energy of photolysis is ~2 eV greater than that of a free H_2O molecule.[70,71] This difference is attributed to the cage effect: in addition to the bond dissociation energy, kinetic energy necessary to overcome the activation barrier at the cage wall is required to spatially separate the fragments.[70,71] In SiO_2 glass, it is expected that the glass network surrounding an SiOH group serves as a barrier to the separation of photogenerated H^0 from NBOHC. Thus it is most likely that the cage effect is responsible for a small Φ (~0.1–0.2) of the photolysis of SiO—H bonds in SiO_2 glass (Fig. 3) compared to the case of O—H bonds in free molecules.

The kinetics of the dimerization of H^0 has been studied intensively in the gas phase.[72,73] These observations indicate that the dimerization of H^0 is a triple collision that involves a

third body, M, which take excess energy (heat of reaction) away from the reaction intermediate,

$$H^0 + H^0 + M \rightarrow H_2 + M. \quad (26)$$

The yield of H_2 is very small unless M is present, whereas the dimerization readily occurs in SiO_2 glass with a large branching ratio for the dimerization $(1-p_I \sim 0.20)$. Evidently, the most probable mechanism is inelastic collisions of the reaction intermediate with Si and O atoms of the glass network,[74] that serve the role of M. This mechanism is similar to that of the formation of H_2 in space, where the surface of interstellar dust particles catalyzes the dimerization of H^0.[75]

The observed ratio of the capture radii of H^0 to NBOHC $(r_3/r_1 = 0.095/0.5 \sim 0.2)$, calculated from the branching ratio of reactions Eqs. (1) and (3), is less than half of the ratio of the atomic radii of H to O (~0.5). This discrepancy is possibly caused by the oversimplification introduced by defining r_3 as a classical "capture radius" within which the reaction probability is 1 and with no reaction occurring at greater separations. In reality, the dimerization may occur at separations greater than r_3. However, the reaction intermediate often redissociates into two H^0s before losing the excess energy to the surrounding Si—O cage.

Figures 10(a) and 10(b) show Arrhenius plots of the diffusion coefficients of H^0 and H_2 in SiO_2 glass, calculated by substituting D_0 and E_a values determined in Secs. III E and III F into Eq. (10). Because of the distribution of the diffusion coefficient, the D-T relation defines an area in the plot rather than a line. The D-T areas of ranges I, II, and III are described using characteristic values of $w(E_a)$ defined by Eqs. (12)–(14). Bold solid lines denote D values calculated at E_a^{max}, while thin solid lines represent those calculated at $E_a^{HM\text{-}low}$ (upper line) and $E_a^{HM\text{-}high}$ (lower line). The degree of separation between the upper and lower thin lines is a measure of the distribution of diffusivity associated with the structural disorder of SiO_2 glass. Results taken from Refs. 39, 40, and 43 (H^0) and Refs. 13, 19, 27, 30, 33, and 35 (H_2) are shown for comparison.

One can introduce an "average" diffusion coefficient D_{avr}, which is the integration of dispersed D values using $w(E_a)$ as the weighting function,

$$D_{avr} = \int_0^\infty D_0 \exp(-E_a/kT) w(E_a) dE_a. \quad (27)$$

The first Fick's equation characterized by D_{avr} of this form is equivalent to a physical model, in which particles starting from a "common" pool can diffuse along many independent and mutually noncrossing diffusion paths, each with a different diffusion coefficient $D(E_a)$ and entrance probability $w(E_a)$. In this model, the "easy" paths with lower activation energy will effectively short-circuit the "difficult" paths.

The dotted lines in Fig. 10 indicate the temperature dependence of D_{avr}. For range I, this line is located far above the bold line, even outside the area defined by the thin lines. This result is due to a high ratio of FWHM to peak energy of $w(E_a)$ $[(E_a^{HM\text{-}high} - E_a^{HM\text{-}low})/E_a^{max} \sim 0.7]$ combined with an extended tail on the low-E_a side. The large difference between D_{avr} and $D(E_a^{max})$ indicates that the physical model underlying D_{avr}, namely, the availability of all diffusion paths within $w(E_a)$ for diffusing particles,[76] does not correspond to the present experimental situation. There is no steady flow of H^0 in either the isothermal or thermal decay experiments, where H^0 is converted to H_2 [Eq. (3)] or captured by radiation-induced NBOHC [Eq. (1)] or E' centers. In these situations, H^0s with high mobility (small E_a) generally react first. This leads to a time-dependent decrease in D_{avr} for the remaining ensemble of H^0s, which approaches $D(E_a^{max})$ with time and even decreases beyond $D(E_a^{max})$ at high temperatures. Thus both the distribution of the diffusion coefficient and its time-dependent decrease affect the diffu-

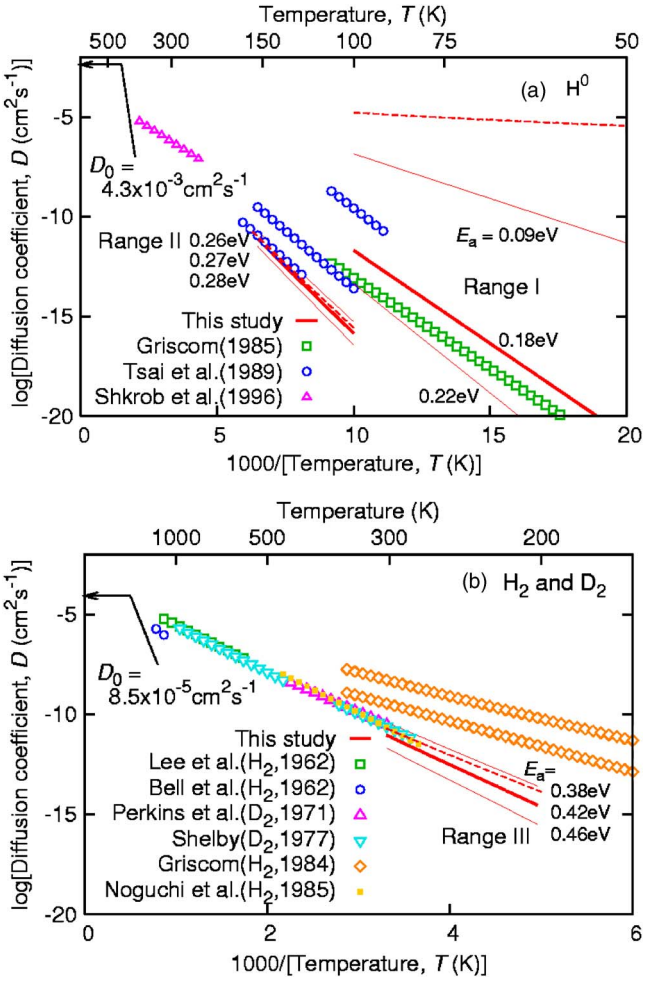

FIG. 10. (Color online) Arrhenius plots of the diffusion coefficients of (a) H^0 and (b) H_2 and D_2. Thick solid lines denote the diffusion coefficients calculated with activation energy E_a values that correspond to the respective maxima of the distributions $w(E_a)$ in Fig. 9 (E_a^{max}), while thin solid lines denote the diffusion coefficients calculated at E_a values at both half maximum points of $w(E_a)$ ($E_a^{HM\text{-}high}$ and $E_a^{HM\text{-}low}$). The dotted lines indicate the average diffusion coefficients D_{avr} calculated by integrating the diffusion coefficient over the $w(E_a)$ distribution [Eq. (27)]. This represents the diffusion coefficient for a steady-state flow that maintains a constant concentration of diffusing species. Results taken from Refs. 39, 40, and 43 (H^0) and Refs. 13, 19, 27, 30, 33, and 35 (H_2) are also shown.

sion of H^0 in SiO_2 glass. This may explain the discrepancy between the various reported *D-T* relations for H^0 [Fig. 10(a)].

The distribution of the diffusion coefficient of H_2 in range III is symmetric, and the FWHM to peak-energy ratio $[(E_a^{\text{HM-high}}-E_a^{\text{HM-low}})/E_a^{\max}\sim 0.2]$ is much smaller than that for H^0 in range I. Hence D_{avr} (dotted line) is located close to $D(E_a^{\max})$ (bold line) [Fig. 10(b)], and the time-dependent decrease in the diffusion coefficient associated with the reactions with NBOHC is relatively small. D_{avr} evaluated in this study agrees well with the value obtained from the permeation of H_2 through SiO_2 glass plates,[13,30–32,34,35,41] films,[33] and fibers.[19] However, it is smaller than the values reported in Ref. 27, which is the first extensive study of the diffusion of H_2 utilizing the reaction with NBOHC. This difference in D_{avr} may result from excess H_2 in typical samples of "Suprasil 1" silica. Suprasil 1 is manufactured by hydrolyzing silane compounds in an O_2—H_2 flame, which can be the source of interstitial H_2 (see also Sec. II A),[51] and has served as a *de facto* standard representative of wet SiO_2 glass in the majority of previous studies. However, the presence of H_2 in Suprasil 1 was not known in earlier studies. The presence of H_2, which can yield E_a values smaller than the true value, is implied by two observations described in Ref. 27: first, the observation that overnight thermal annealing of the sample in air at 1100 °C greatly suppresses the bleaching step of NBOHC by H_2 (Ref. 77); and second, the observation that the temperature range of this bleaching step ($\sim$200–300 K) approximately coincides with that of range III for the H_2-loaded sample in the present study (Fig. 1, range III).[78]

V. CONCLUSIONS

Photolysis of silanol (SiOH) groups in wet SiO_2 glasses with a single F_2 laser pulse ($\sim$30 mJ cm^{-2}) creates $\sim 10^{16}$ cm^{-3} pairs of oxygen dangling bonds (NBOHC) and mobile hydrogen atoms (H^0). We quantitatively studied the formation, diffusion, and diffusion-limited reactions of H^0 and hydrogen molecules (H_2) in SiO_2 glass between 10 and 330 K by analyzing the time- and temperature-dependent changes in NBOHC concentration. We also examined the influence of the SiO_2 glass network on these processes. The observed quantum yield of photolysis of SiO—H bonds (0.15 ± 0.05) is smaller than that measured for O—H bonds of molecules in a gaseous phase ($\sim$1), suggesting that some of the H^0s created by the photolysis cannot escape from NBOHC due to the cage effect, i.e., collisions of H^0 with the glass network surrounding NBOHC. A significant number of the photogenerated H^0 reacts with other H^0s to form H_2, and the energy loss of the reaction intermediate through its collisions with the glass network is crucial in generating H_2 by this mechanism. The branching ratio between the dimerization of H^0 and the reaction of H^0 with NBOHC depends on the ratio of the capture radii of H^0 and NBOHC, but is not dependent on the initial concentration and diffusion coefficient of H^0. Thus the yield of H_2 due to the dimerization is independent of temperature and the method of H^0 creation if the capture radii remain constant and multiple annihilation-regeneration processes of H^0 do not occur. The diffusion coefficients of H^0 and H_2 were obtained from the concentration changes of NBOHC with the aid of a numerical simulation. A variety of sizes and shapes of interstitial voids induces a distribution of the diffusion coefficients of H^0 and H_2. Consequently, H^0 and H_2 with high mobilities disappear faster than those with low mobilities. This results in a time-dependent decrease in the average diffusion coefficient. Since the distribution of the diffusion coefficient of H^0 is very broad, the average diffusion coefficient of H^0 decreases considerably with time. In contrast, the distribution of the diffusion coefficient of H_2 is relatively narrow, and its average value agrees well with data from permeation experiments.

*Corresponding author. Email address: kaji2@lucid.msl.titech.ac.jp

[1] S. P. Faile and D. M. Roy, Mater. Res. Bull. **5**, 385 (1970).
[2] S. Yamagata, Mineral. J. **15**, 333 (1991).
[3] V. A. Radzig, V. N. Bagratashvili, S. I. Tsypina, P. V. Chernov, and A. O. Rybaltovskii, J. Phys. Chem. **99**, 6640 (1995).
[4] D. R. Sempolinski, T. P. Seward, C. Smith, N. Borrelli, and C. Rosplock, J. Non-Cryst. Solids **203**, 69 (1996).
[5] P. Karlitschek, G. Hillrichs, and K. F. Klein, Opt. Commun. **155**, 376 (1999).
[6] M. Shimbo, T. Nakajima, N. Tsuji, T. Kakuno, and T. Obara, Jpn. J. Appl. Phys., Part 2 **38**, L848 (1999).
[7] C. M. Smith, N. F. Borrelli, and R. J. Araujo, Appl. Opt. **39**, 5778 (2000).
[8] M. Oto, S. Kikugawa, N. Sarukura, M. Hirano, and H. Hosono, IEEE Photonics Technol. Lett. **13**, 978 (2001).
[9] M. Oto, S. Kikugawa, T. Miura, M. Hirano, and H. Hosono, J. Non-Cryst. Solids **349**, 133 (2004).
[10] H. Hosono, Y. Abe, H. Imagawa, H. Imai, and K. Arai, Phys. Rev. B **44**, 12043 (1991).
[11] H. Imai, K. Arai, H. Hosono, Y. Abe, T. Arai, and H. Imagawa, Phys. Rev. B **44**, 4812 (1991).
[12] S. P. Faile and D. M. Roy, J. Am. Ceram. Soc. **54**, 533 (1971).
[13] T. Bell, G. Hetherington, and K. H. Jack, Phys. Chem. Glasses **3**, 141 (1962).
[14] J. M. Wiesenfeld, J. Stone, D. Marcuse, C. A. Burrus, and S. Yang, J. Appl. Phys. **61**, 5447 (1987).
[15] B. C. Schmidt, F. M. Holtz, and J.-M. Beny, J. Non-Cryst. Solids **240**, 91 (1998).
[16] K. Mochizuki, Y. Namihira, and H. Yamamoto, Electron. Lett. **19**, 743 (1983).
[17] N. Uesugi, Y. Murakami, C. Tanaka, Y. Ishida, Y. Mitsunaga, Y. Negishi, and N. Uchida, Electron. Lett. **19**, 762 (1983).
[18] T. Tanifuji, M. Matsumoto, M. Tokuda, and M. Miyauchi, Electron. Lett. **20**, 13 (1984).
[19] K. Noguchi, N. Shibata, N. Uesugi, and Y. Negishi, J. Lightwave Technol. **LT-3**, 236 (1985).

[20] J. Stone, J. Lightwave Technol. **LT-5**, 712 (1987).
[21] Y. Ikuta, K. Kajihara, M. Hirano, and H. Hosono, Appl. Opt. **43**, 2332 (2004).
[22] T. A. Michalske and S. W. Freiman, J. Am. Ceram. Soc. **66**, 284 (1983).
[23] B. C. Bunker, J. Non-Cryst. Solids **179**, 300 (1994).
[24] J. E. Shelby, J. Appl. Phys. **50**, 3702 (1979).
[25] C. M. Smith, N. F. Borrelli, J. J. Price, and D. C. Allan, Appl. Phys. Lett. **78**, 2452 (2001).
[26] E. M. Birtch and J. E. Shelby, J. Non-Cryst. Solids **349**, 156 (2004).
[27] D. L. Griscom, J. Non-Cryst. Solids **68**, 301 (1984).
[28] M. Vitiello, N. Lopez, F. Illas, and G. Pacchioni, J. Phys. Chem. A **104**, 4674 (2000).
[29] R. M. Barrer, J. Chem. Soc. **136**, 378 (1934).
[30] R. W. Lee, R. C. Frank, and D. E. Swets, J. Chem. Phys. **36**, 1062 (1962).
[31] R. W. Lee, J. Chem. Phys. **38**, 448 (1963).
[32] B. Wu, J. Vac. Sci. Technol. B **24**, 1 (2006).
[33] W. G. Perkins and D. R. Begeal, J. Chem. Phys. **54**, 1683 (1971).
[34] J. E. Shelby and S. C. Keeton, J. Appl. Phys. **45**, 1458 (1974).
[35] J. E. Shelby, J. Appl. Phys. **48**, 3387 (1977).
[36] A. R. Silin and L. N. Skuja, J. Mol. Struct. **61**, 145 (1980).
[37] K. L. Brower, P. M. Lenahan, and P. V. Dressendorfer, Appl. Phys. Lett. **41**, 251 (1982).
[38] T. Miyazaki, N. Azuma, and K. Fueki, J. Am. Ceram. Soc. **67**, 99 (1984).
[39] D. L. Griscom, J. Appl. Phys. **58**, 2524 (1985).
[40] T. E. Tsai, D. L. Griscom, and E. J. Friebele, Phys. Rev. B **40**, 6374 (1989).
[41] Y. Morimoto, T. Igarashi, H. Sugahara, and S. Nasu, J. Non-Cryst. Solids **139**, 35 (1992).
[42] K. Vanheusden, W. L. Warren, R. A. B. Devine, D. M. Fleetwood, J. R. Schwank, M. R. Shaneyfelt, P. S. Winokur, and Z. J. Lemnios, Nature (London) **386**, 587 (1997).
[43] I. A. Shkrob and A. D. Trifunac, Phys. Rev. B **54**, 15073 (1996).
[44] E. Hörnlund and G. Hultquist, J. Appl. Phys. **94**, 4819 (2003).
[45] M. Cannas, S. Costa, R. Boscaino, and F. M. Gelardi, J. Non-Cryst. Solids **337**, 9 (2004).
[46] N. Leclerc, C. Pfleiderer, H. Hitzler, J. Wolfrum, K.-O. Greulich, S. Thomas, H. Fabian, R. Takke, and W. Englisch, Opt. Lett. **16**, 940 (1991).
[47] N. Leclerc, C. Pfleiderer, H. Hitzler, J. Wolfrum, K.-O. Greulich, S. Thomas, and W. Englisch, J. Non-Cryst. Solids **149**, 115 (1992).
[48] C. Mühlig, W. Triebel, S. Bark-Zollmann, and D. Grebner, Nucl. Instrum. Methods Phys. Res. B **166-167**, 698 (2000).
[49] F. Messina and M. Cannas, J. Phys.: Condens. Matter **17**, 3837 (2005).
[50] K. Kajihara, L. Skuja, M. Hirano, and H. Hosono, Appl. Phys. Lett. **79**, 1757 (2001).
[51] K. Kajihara, L. Skuja, M. Hirano, and H. Hosono, Phys. Rev. Lett. **89**, 135507 (2002).
[52] H. Imai, K. Arai, T. Saito, S. Ichimura, H. Nonaka, J. P. Vigouroux, H. Imagawa, H. Hosono, and Y. Abe, in *The Physics and Technology of Amorphous* SiO_2, edited by R. A. B. Devine (Plenum Press, New York, 1988), pp. 153–159.
[53] K. Awazu and H. Kawazoe, J. Non-Cryst. Solids **179**, 214 (1994).
[54] Y. Morimoto, S. Nozawa, and H. Hosono, Phys. Rev. B **59**, 4066 (1999).
[55] K. Kajihara, M. Hirano, L. Skuja, and H. Hosono, Phys. Rev. B **72**, 214112 (2005).
[56] K. Kajihara, Y. Ikuta, M. Oto, M. Hirano, L. Skuja, and H. Hosono, Nucl. Instrum. Methods Phys. Res. B **218**, 323 (2004).
[57] H. Hosono, Y. Ikuta, T. Kinoshita, K. Kajihara, and M. Hirano, Phys. Rev. Lett. **87**, 175501 (2001).
[58] L. N. Skuja and A. R. Silin, Phys. Status Solidi A **70**, 43 (1982).
[59] M. Stapelbroek, D. L. Griscom, E. J. Friebele, and G. H. Sigel, Jr., J. Non-Cryst. Solids **32**, 313 (1979).
[60] L. Skuja, H. Hosono, and M. Hirano, Proc. SPIE **4347**, 155 (2001).
[61] M. Mizuguchi, L. Skuja, H. Hosono, and T. Ogawa, Opt. Lett. **24**, 863 (1999).
[62] T. R. Waite, Phys. Rev. **107**, 463 (1957).
[63] K. Kajihara, M. Hirano, L. Skuja, and H. Hosono, J. Non-Cryst. Solids **352**, 2307 (2006).
[64] H. R. Philipp, in *Handbook of Optical Constants of Solids*, *Academic Press Handbook Series*, edited by E. D. Palik (Academic Press, Orlando, 1985), p. 749.
[65] L. Skuja, K. Kajihara, Y. Ikuta, M. Hirano, and H. Hosono, J. Non-Cryst. Solids **345 & 346**, 328 (2004).
[66] L. Skuja, K. Kajihara, M. Hirano, and H. Hosono, in *Proceedings of the 20th International Congress on Glass, Kyoto, 2004*, p. O-14-052.
[67] L. Skuja, K. Kajihara, M. Hirano, A. Saitoh, and H. Hosono, J. Non-Cryst. Solids **352**, 2297 (2006).
[68] X. F. Yang, D. W. Hwang, J. J. Lin, and X. Ying, J. Chem. Phys. **113**, 10597 (2000).
[69] S. Satyapal, J. Park, R. Bersohn, and B. Katz, J. Chem. Phys. **91**, 6873 (1989).
[70] R. Schriever, M. Chergui, H. Kunz, V. Stepanenko, and N. Schwentner, J. Chem. Phys. **91**, 4128 (1989).
[71] E. I. Tarasova, A. M. Ratner, V. M. Stepanenko, I. Y. Fugol, M. Chergui, R. Schriever, and N. Schwentner, J. Chem. Phys. **98**, 7786 (1993).
[72] F. S. Larkin, Can. J. Chem. **46**, 1005 (1968).
[73] D. W. Trainor, D. O. Ham, and F. Kaufman, J. Chem. Phys. **58**, 4599 (1973).
[74] K. Kajihara, M. Hirano, L. Skuja, and H. Hosono, J. Am. Chem. Soc. **128**, 5371 (2006).
[75] L. Hornekær, A. Baurichter, V. V. Petrunin, D. Field, and A. C. Luntz, Science **302**, 1943 (2003).
[76] The calculated values of $D_{avr}(T)$ can be meaningful in a different case, a permeation experiment, where the concentration of diffusing particles is not time dependent and each particle can take any diffusion path, including ones with low activation energies.
[77] In wet SiO_2 glass thermally annealed at high temperatures, SiOH groups are most likely to be removed by the reaction $2SiOH \rightarrow Si—O—Si + H_2O$, rather than $2SiOH \rightarrow Si—O—O—Si + H_2$ (Ref. 79). Thus the thermal annealing at 1100 °C described in Ref. 27 is unlikely to produce numerous peroxy linkages Si—O—O—Si, that are considered to trap mobile H^0, prevent the formation of H_2, and consequently suppress the bleaching step of NBOHC by H_2. Interstitial O_2 may serve as another source of oxygen-related H_2 traps (Refs. 80–82); up to $\sim 4 \times 10^{15}$ cm^{-3} O_2 can be incorporated in wet SiO_2 glass by thermal annealing in air at 1100 °C (Ref. 83). However, this is also unlikely to be the main factor in the disappearance of the bleaching step because the saturation concentration of O_2 is comparable to the concentrations of other hydrogen traps (NBOHC and

E' centers). On the other hand, the annealing conditions described in Ref. 27 were sufficient for the removal of interstitial H_2 (Refs. 13 and 30).

[78] In Fig. 2(a) of Ref. 27, the early stage of the NBOHC bleaching step by H_2 is well reproduced by a simulation that assumes the presence of excess H_2 ($[H_2]/[NBOHC]=400$) at $E_a=0.45$ eV.

[79] R. H. Doremus, *Diffusion of Reactive Molecules in Solids and Melts* (John Wiley & Sons, New York, 2002).

[80] J. E. Shelby, J. Appl. Phys. **51**, 2589 (1980).

[81] J. E. Shelby, J. Non-Cryst. Solids **179**, 138 (1994).

[82] K. Kajihara, M. Hirano, L. Skuja, and H. Hosono, J. Appl. Phys. **98**, 043515 (2005).

[83] K. Kajihara, H. Kamioka, M. Hirano, T. Miura, L. Skuja, and H. Hosono, J. Appl. Phys. **98**, 013529 (2005).